

## Lattice Boltzmann Simulation of Cavitating Flows

Giacomo Falcucci<sup>1,\*</sup>, Stefano Ubertini<sup>2</sup>, Gino Bella<sup>3</sup> and Sauro Succi<sup>4</sup>

<sup>1</sup> *Department of Technologies, University of Naples "Parthenope", Centro Direzionale - Isola C4, 80143 Naples, Italy.*

<sup>2</sup> *DEIM - Industrial Engineering School, University of Tuscia, Largo dell'Università s.n.c., 01100, Viterbo, Italy.*

<sup>3</sup> *Department of Mechanical Engineering, University of "Tor Vergata", Viale Politecnico, Rome, Italy.*

<sup>4</sup> *Istituto per le Applicazioni del Calcolo - CNR, Via dei Taurini, 00100 Roma, Italy.*

Received 29 October 2011; Accepted (in revised version) 27 January 2012

Available online 29 August 2012

---

**Abstract.** The onset of cavitating conditions inside the nozzle of liquid injectors is known to play a major role on spray characteristics, especially on jet penetration and break-up. In this work, we present a Direct Numerical Simulation (DNS) based on the Lattice Boltzmann Method (LBM) to study the fluid dynamic field inside the nozzle of a cavitating injector. The formation of the cavitating region is determined via a multi-phase approach based on the Shan-Chen equation of state. The results obtained by the LBM simulation show satisfactory agreement with both numerical and experimental data. In addition, numerical evidence of bubble break-up, following upon flow-induced cavitation, is also reported.

**PACS:** 47.11.-j, 47.65.Cb

**Key words:** Lattice Boltzmann, multiphase flows, cavitation, liquid spray, nozzle.

---

## 1 Introduction

The use of some form of liquid sprays is very common in industrial processes. Therefore, there is a constant demand and a very high scientific interest in liquid atomization, as the spray characteristics are crucial to the success of the particular industrial application. A remarkable example is represented by direct injection internal combustion engines, whose efficiency and pollutant emissions are significantly affected by the fuel spray characteristics [1, 2]. However, the understanding and the numerical simulation of liquid

---

\*Corresponding author. *Email addresses:* giacomo.falcucci@uniparthenope.it (G. Falcucci), stefano.ubertini@uniparthenope.it (S. Ubertini), bella@uniroma2.it (G. Bella), succi@iac.cnr.it (S. Succi)

spray formation is a very challenging task as it involves several complex phenomena. A liquid spray is a collection of fine liquid dispersed droplets generated by injecting a liquid fuel in a gaseous environment (i.e. fuel spray in an engine cylinder) through a nozzle. The flow conditions inside the nozzle are deeply influenced by both injection pressure and nozzle dimensions. Under particular conditions, as for example in diesel injection systems, liquid velocity inside the nozzle may be very high and the static pressure may locally drop below vapor pressure, leading to *cavitation*, which is to say the formation of cavities or gas bubbles in the liquid. The simulation of this phenomenon is a very challenging task, but is crucial for a proper modeling of the subsequent spray. Experimental works in literature, in fact, have demonstrated that the rising of cavitation significantly influences the atomization process of a liquid spray [3–6]. On the other hand, due to the complexity of the involved phenomena, only few theoretical and numerical studies of nozzle flow cavitation are available in literature [7].

The aim of this work is to test the Lattice Boltzmann Method (LBM) as a possible candidate to study the onset of cavitation inside a nozzle. LBM is a numerical method to investigate fluid dynamic fields; it is not based on the continuum assumption as the Navier-Stokes (NS) approach, but rather on the notion of particle distribution functions, as developed Boltzmann's kinetic theory. In recent years, LBM has been successfully employed to study both single-phase fluid dynamics and complex phenomena, like multiphase/reacting flows [8–11], fluid-structure interaction [12], and also bubble cavitation [13, 14].

In a recent work, the authors successfully employed the LBM to model the break-up of a liquid spray [15], for different values of Reynolds and Weber numbers. The multiphase nature of the flow has been modeled through the approach proposed by Shan and Chen [16, 17]. In this work, LBM coupled to Shan-Chen model is employed to simulate the flow and the onset of cavitation inside a nozzle with simplified geometry under realistic conditions, including the dynamics of the injector pintle. To the best of our knowledge, this is the first Direct Numerical Simulation (DNS) of a flow-induced cavitation using the LB method.

Different cavitation phenomena are reproduced, depending on the dynamic schedule of the injector; in particular for the case where such dynamics takes into account the fluid and pintle inertia, cavitation is found to be followed by break-up phenomena in the nozzle.

## 2 Numerical method

The Lattice Boltzmann Method (LBM) is a numerical approach to investigate fluid dynamic phenomena based on a minimal discrete form of Boltzmann's kinetic equation [18]. The basic equation of this method reads as follows,

$$f_i(\vec{r} + \vec{c}_i \delta t; t + \delta t) - f_i(\vec{r}, t) = -\omega \delta t (f_i - f_i^{eq}) + F_i \delta t \quad (2.1)$$

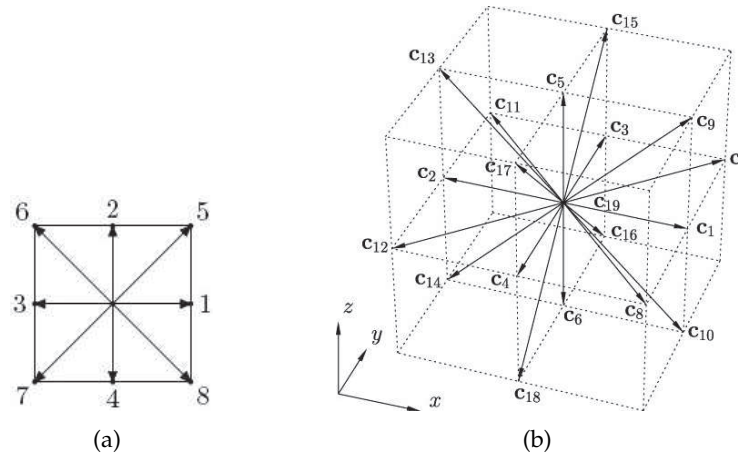


Figure 1: Sketch of two typical lattices: (a) two dimensional, 9 speed-directions or  $D2Q9$  lattice; (b) three dimensional, 19 speed-directions or  $D3Q19$  lattice. Both lattices include a rest particle.

in which  $i$  represents the set of discrete speeds. The left hand side of Eq. (2.1) describes the streaming of force-free particles, where, in line with the mesoscopic nature of the LB model, each particle represents a mesoscopic collection of physical molecules. The first term at the RHS describes collisional interactions, in the form of a simple relaxation towards a local equilibrium,  $f_i^{eq}$ , in a time lapse  $\tau = 1/\omega$ . The second term on the RHS describes the sources of mass, momentum and energy resulting the coupling of the fluid with the environment. For simplicity, a simple single-time relaxation form, also known as Bhatnagar-Gross-Krook (BGK) [19, 20] is used, although more sophisticated multi-relaxation scattering matrix models are also available [21].

Following the Chapman-Enskog asymptotic expansion, the LBE can be shown to reproduce the dynamics of an incompressible flow, whose density and velocity are given by:

$$\rho(\vec{r}, t) = \sum_i f_i(\vec{r}, t), \quad (2.2)$$

$$u(\vec{r}, t) = \frac{1}{\rho(\vec{r}, t)} \sum_i c_i f_i(\vec{r}, t). \quad (2.3)$$

The local equilibria  $f_i^{eq}$  in Eq. (2.1) are typically chosen in the form of a second-order expansion in the local mach number,  $Ma = u/c_s$ , of the local Maxwell distribution [20]:

$$f_i^{eq}(\vec{r}; t) = w_i \rho \left( 1 + \frac{\vec{u} \cdot \vec{c}_i}{c_s^2} + \frac{(\vec{u} \cdot \vec{c}_i)^2}{2c_s^4} - \frac{\vec{u} \cdot \vec{u}}{2c_s^2} \right). \quad (2.4)$$

Finally,  $w_i$  is a set of discrete weights obeying the following normalizations,  $\sum_i w_i = 1$ ,  $\sum_i w_i c_{ix}^2 = \sum_i w_i c_{iy}^2 = c_s^2 = 1/3$ ,  $c_s$  being the lattice speed of sound.

Since all fluid variables are defined in terms of kinetic moments of the discrete distribution, see Eqs. (2.2) and (2.3), the discrete forcing  $F_i$  can be designed in weak-form,

i.e. by matching its contributions to mass-momentum and momentum-flux, to those of a continuum source term in the form  $S_u = \vec{F}/m \cdot \partial f / \partial \vec{u}$  [18].

This yields

$$F_i = w_i \frac{\vec{F} \cdot \vec{c}_i}{c_s^2}. \quad (2.5)$$

This uniquely specifies the discrete forcing in terms of the desired continuum force per unit volume  $\vec{F}$ . In actual practice, it is known that a more efficient and stable implementation of this force consists of using a shifted flow velocity in the expression (2.4) of the local equilibria, namely

$$\vec{u} \rightarrow \vec{u}' = \vec{u} + \frac{\vec{F}\tau}{\rho}. \quad (2.6)$$

Since these matters have been described at length in the LB literature, we shall not delve into further details. Instead, we proceed by discussing the specific form of the pseudo-forces/potentials to be employed in the present work.

## 2.1 Shan-Chen: single-range pseudo-potential model

We briefly revisit the main features of the standard, single-range, Shan-Chen model [16, 17].

The Shan-Chen force reads as follows

$$\vec{F}(\vec{r};t) = G\psi(\rho(\vec{r})) \sum_i w_i \vec{c}_i \delta t \psi[\rho(\vec{r} + \vec{c}_i \delta t)], \quad (2.7)$$

where  $G$  parametrizes the strength of the non-ideal interactions between neighbors in the first Brillouin region (*belt*, for simplicity) spanned by the lattice vectors  $\vec{r} + \vec{c}_i \delta t$ .

The pseudo-potential is chosen in the following form

$$\psi(\rho) = \rho_0 (1 - e^{-\rho/\rho_0}), \quad (2.8)$$

where  $\rho_0$  is a reference density (in the practice, usually  $\rho_0 = 1$ ), below which the pseudo-potential  $\psi$  reduces to the ordinary fluid density. In the high-density limit,  $\rho \gg \rho_0$ , the above functional form saturates to a constant value,  $\rho_0$ , so that the associated force becomes vanishingly small. This is required to prevent density collapse under attractive interactions. Indeed, in the Shan-Chen model, phase-separation is triggered by attractive interactions ( $G < 0$ ) between neighbors in the first belt. Attractive interactions enhance density gradients and promote a subsequent progressive steepening of the interface, eventually taking the system to a density collapse. In dense fluids and liquids such density collapse is prevented by hard-core repulsive forces, which stop the indefinite build-up of density gradients, thereby stabilizing the fluid interface. As anticipated above, in the Shan-Chen model, such a stabilizing effect is surrogated by imposing a saturation of the intermolecular attraction for densities above a reference value,  $\rho_0$ .

Despite its simplicity, the Shan-Chen model encodes the two basic features of interacting fluids, namely a non-ideal equation of state and a non-zero surface tension. The former is given by

$$P(\rho) = \rho c_s^2 + \frac{1}{2} G c_s^2 \psi^2 \quad (2.9)$$

and shows a phase transition for  $G < G_{crit} = -4$ . The surface tension is given by

$$\sigma \propto -G c_s^4 \int (\partial_y \psi)^2 \delta y, \quad (2.10)$$

where  $y$  runs across the liquid-vapor interface. To be noted that within this model, the equation of state and surface tension cannot be varied independently. This is easily disposed of by implementing multi-range potentials [9]. In this work, however, we shall confine our attention to single-range potentials.

### 3 Simulations & results

From the thermodynamic point of view, cavitation is the process by which a liquid vaporizes under the effect of a sudden pressure loss, typically due to mechanical flow conditions (see Fig. 2). This is a non-thermal, flow-induced, strongly non-equilibrium phase transition, which is hard to reproduce in a direct numerical simulation, without the use of phenomenological models (i.e. VOF, *bubble-model*, Eulerian-Lagrangian coupling for dispersed phase, etc.) [7, 22], because of the numerical difficulty in tracing the dynamic instability leading to the phase transition. This is a significant advantage of LB multi-phase approach, in which phase transition and the onset of the interface emerge directly from phase-interaction term  $F_i$  in Eq. (2.1).

The operating regime inside a nozzle (e.g. diesel injectors) may be characterized by two dimensionless parameters, the cavitation number, and the discharge number. The former is defined as [23]

$$C_n = \frac{p_{in} - p_{out}}{p_{out} - p_{vap}}, \quad (3.1)$$

where  $p_{in}$  and  $p_{out}$  are the fluid pressure at the inlet and outlet sections, respectively, while  $p_{vap}$  the vapor pressure in equilibrium,  $\rho$  the fluid density and  $U$  a reference velocity. The discharge coefficient is related to the cavitation number by the following relation [24]

$$C_d \sim 0.67 \sqrt{1 + \frac{1}{C_n}}. \quad (3.2)$$

By definition, cavitation occurs at  $C_n > 1$ , whereas the discharge coefficient is a measure of the dissipative effects associated with cavitation phenomena. Ideally, injectors should work at high  $C_n$  and low  $C_d$ , corresponding to the production of highly atomized sprays at a minimum energy cost.

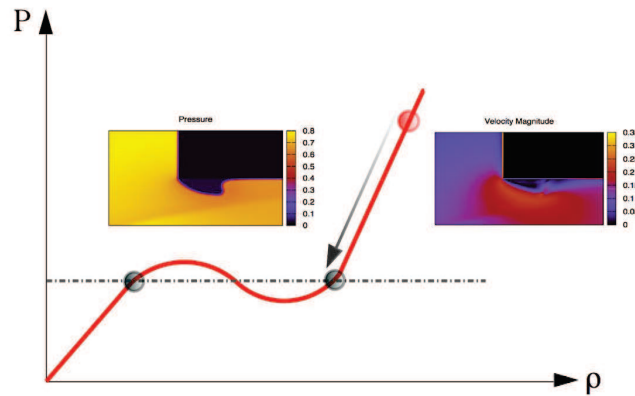


Figure 2: Thermodynamic sketch of flow-induced cavitation: the velocity increase due to the reduction of channel section causes the pressure drop, driving the formation of non-equilibrium vapor bubbles. The snapshots provide a qualitative idea of pressure and velocity fields inside the injector nozzle, in presence of cavitation.

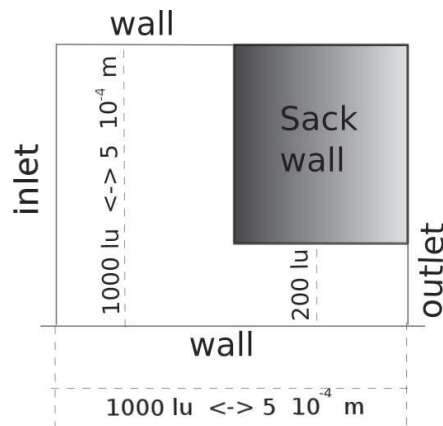


Figure 3: The geometry of the simulation. The fluid flows into the injector from the inlet section and is subsequently channeled into the nozzle duct, where it experiences the acceleration causing the pressure drop which drives the cavitation at the inlet of the nozzle duct.

Our simulations are performed in the two-dimensional computational domain shown in Fig. 3, using  $10^3$  grid points along each dimension and a standard  $D2Q9$  lattice [20]. The inlet condition is fixed by imposing the magnitude of the fluid velocity (flat profile), the outflow is a “zero-gradient” condition and the walls are all *no-slip*, i.e. zero velocity. The inlet velocity is either a step function or a linear ramp-up function of time, corresponding to a sudden and gradual opening of the nozzle, respectively. The corresponding velocity time schedules are shown in Fig. 4.

The main parameters of the simulation set-up are given in Table 1.

With these reference values, we find  $p \sim 0.043$ ,  $p_{vap} \sim 0.015$ , corresponding to a cavitation number is of the order of  $C_n \sim \frac{0.043 - 0.015}{0.0169} \sim 1.65$ , the regime of incipient cavitation.

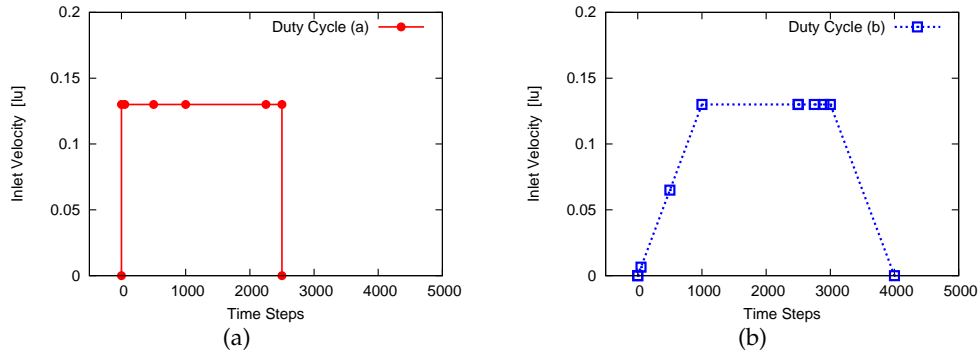


Figure 4: Time-schedule of the two considered inlet velocities. The dots correspond to time instants associated with the snapshots of density and pressure, as shown in the subsequent figures.

Table 1: Flow characteristics.

Reynolds number at inlet section, $Re$	$\sim 780$	
Weber number at inlet section, $We$	$\sim 600$	
$G$ parameter in the Shan-Chen EOS	$-5.0$	
liquid phase density	1.92	lu
vapour phase density (combustion chamber)	0.05	lu
liquid/gas density ratio	$\sim 38$	
surface tension	0.056	lu
liquid phase inlet velocity	0.13	lu
nozzle radius	200	lu
grid spacing	$2.5 \cdot 10^{-7}$	m
total grid nodes	$10^6$	

### 3.1 Constant inlet velocity

In Fig. 5, we report a time sequence of the density and pressure at  $t = 50, 500, 1000$ , for the case of constant inlet velocity. From this sequence, the onset of a cavitating region at the entrance of the nozzle can be observed. The cavitation number and the discharge coefficients for this case are  $C_n = 1.65$  and  $C_d = 0.83$ , respectively. The dynamic morphology of the cavitation bubble appears to be in satisfactory agreement with previous numerical work, as well as experimental observations [7, 25].

In Fig. 6, we report the density configuration and corresponding velocity profiles at a later stage of the evolution,  $t = 2250$ . As one can appreciate, the cavitation bubble ruptures under the effect of the local fluid flow, which exhibits a coherent vortex right after the entrance of the nozzle, as visible from panel b) of Fig. 6, reporting the associated flow velocity pattern at the same time instant. This is consistent with the values of the local Reynolds  $Re = U_{in} D / \nu \sim 800$  and Weber  $We = \rho U_{in}^2 D / \sigma \sim 600$  numbers, both values being based on the height of the inlet duct. Since the Weber number measures the propensity

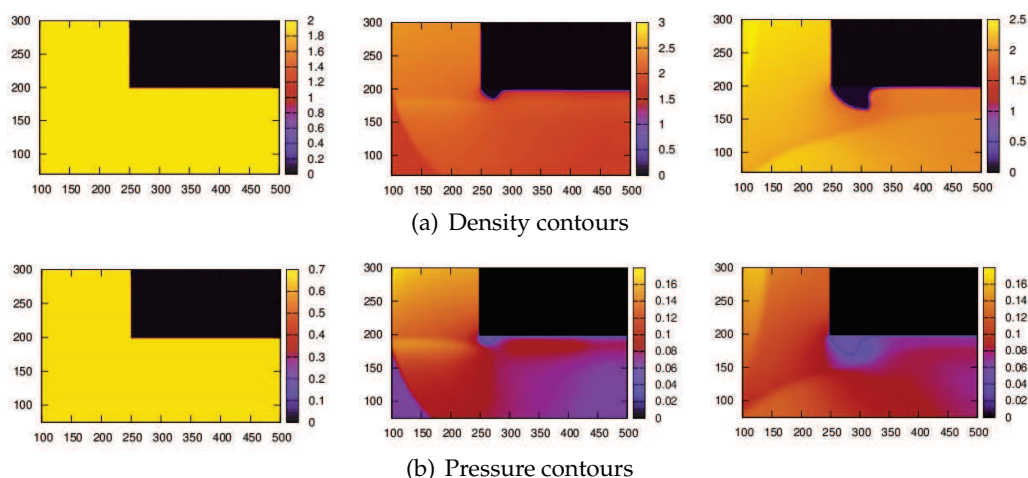


Figure 5: Density (top panel) and pressure (bottom panel) configuration for the case of constant inlet velocity, at  $t=50, 500, 1000$ . The formation of a cavitation bubble at the inlet of the nozzle duct is well visible. The corresponding pressure drop in correspondence of the bubble is also well visible from the contours in the bottom panel. The axes report  $X$  and  $Y$  coordinates of the computational domain.

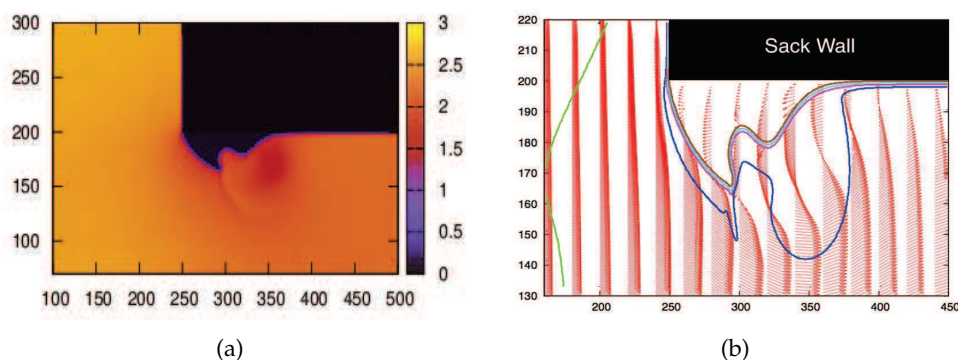


Figure 6: Rupture of the cavitation bubble at  $t=1250$ : (a) density contours, (b) density iso-contours juxtaposed to velocity vectors. The local cavitation number is  $C_{II} \sim 1.65$ . Locally inverted velocity profiles in correspondence with the bubble position, are clearly visible. They are most likely bearing a significant contribution to the rupture of the bubble. The axes report  $X$  and  $Y$  coordinates of the computational domain.

of droplets/bubbles to deform under fluid flow, one should more appropriately define it in terms of actual size of the bubble rather than the inlet diameter, leading to a much smaller value, of the order of  $We \sim 10$ , still large enough to allow significant deformations and possibly breakup.

### 3.2 Dynamic inlet velocity

In Fig. 7, we report the same time sequence as above of the density and pressure distribution for the case of dynamic inlet velocity, typical of engine injection strategies. The main

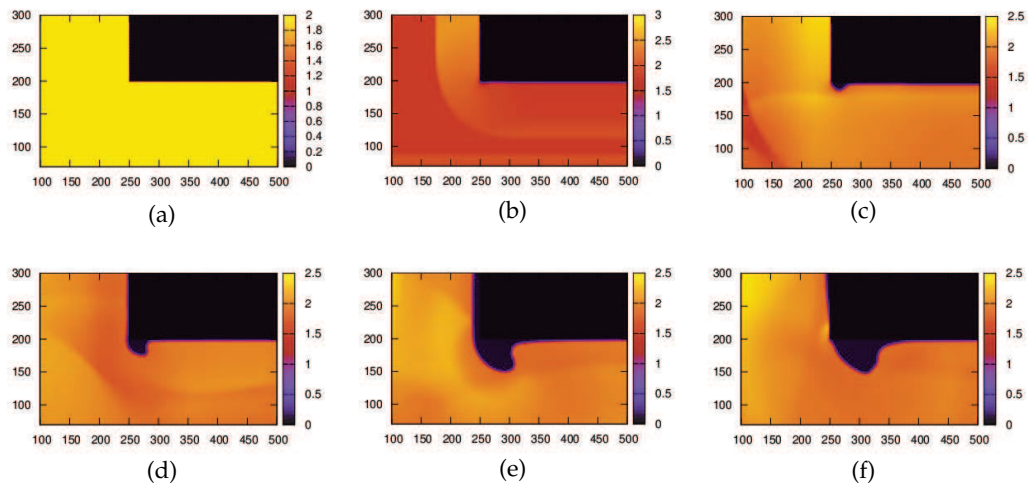


Figure 7: Density configuration for the case of dynamic inlet velocity, at  $t=50,250,500,750,1000,1250$  (a-f). The formation of a cavitating region on the vertical wall of the sack is evident from panels (e) and (f). The axes report  $X$  and  $Y$  coordinates of the computational domain.

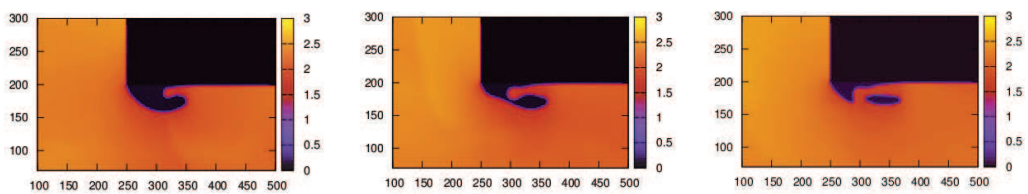


Figure 8: Rupture of cavitation bubble with dynamic inlet velocity, at  $t=2500,2750,2900$ , i.e. within the flat-top in Fig. 4(b). The breakup and consequent separation of a daughter bubble is apparent. The axes report  $X$  and  $Y$  coordinates of the computational domain.

feature, as compared to the case in the previous section, is the formation of a cavitating region on the vertical wall of the sack. This is in line with previous numerical findings, where the inertia of the pintle was taken into account [26].

Finally, in Fig. 8, we show the density and pressure contours for the same case but at a later stage,  $t=2500, 2750, 2900$ , corresponding to the flat-top of the inlet velocity profile in Fig. 4(b). Remarkably, at variance with the case of constant inlet velocity, the cavitation bubble not only shows rupture, but also gives rise to a secondary bubble (break-up), which is then entrained by the mainstream flow. Since the basic parameters, and most notably the cavitation number, are exactly the same as for the case in the previous section, we conclude that the rupture of the bubble is a result of the dynamic schedule of the inlet velocity. At the moment, we have no firm explanation for this dynamical phenomenon.

The presence of such secondary bubbles is of utmost practical importance for the operation of the injector, since it is known that they have a major impact on spray formation and break up at the nozzle exit [6, 7, 27].

## 4 Conclusions

Summarizing, we have used the Shan-Chen model for the computational study of cavitation phenomena inside the nozzle of a liquid injector, including static and dynamic injection strategies. Cavitation is observed under all conditions, and, in the case of dynamic inlet velocity, break-up phenomena are also detected. To the best of our knowledge, this is the first time that such flow-induced cavitation and break-up phenomena are observed in direct simulation of multi-phase flows using LB. Future studies will explore the dependence of the dynamic morphology of the bubbles on the details of the intermolecular interactions [9] and on the nozzle geometry.

## Acknowledgments

We thank Prof. H.A. Stone for his valuable comments and criticism.

## References

- [1] G. Stiesch. *Modeling Engine Spray and Combustion Processes*. Springer-Verlag, Heidelberg, 2003.
- [2] E. Giannadakis, D. Papoulias, M. Gavaises, C. Arcoumanis, C. Sotiriou, and W. Tang. Evaluation of the predictive capability of diesel nozzle cavitation models. SAE Tech. Paper 2007-01-0245, 2007.
- [3] H. Afzal, C. Arcoumanis, M. Gavaises, and N. Kampanis. Internal flow in diesel injector nozzles: Modelling and experiments. IMechE, pp. S492/S2/99, 1999.
- [4] H. Roth, M. Gavaises, and C. Arcoumanis. Cavitation initiation, its development and link with flow turbulence in Diesel injector nozzles. SAE Tech. Paper 2002-01-0214, 2002.
- [5] N. Tamaki, M. Shimizu, K. Nishida, and H. Hiroyasu. Effects of cavitation and internal flow on atomization of a liquid jet. *Atomization and Sprays*, 8(2):179–197, 1998.
- [6] C. Arcoumanis, M. Badami, H. Flora, and M. Gavaises. Cavitation in real-size multi-hole diesel injector nozzles. SAE Trans. J. Engines, 109(3):1485–1500, 2000.
- [7] E. Giannadakis, M. Gavaises, and C. Arcoumanis. Modelling of cavitation in diesel injector nozzles. *J. Fluid Mech.*, 616:153–193, 2008.
- [8] S. Chibbaro, G. Falcucci, G. Chiatti, H. Chen, X. Shan, and S. Succi. Lattice Boltzmann models for nonideal fluids with arrested phase-separation. *Phys. Rev. E*, 77:036705, 2008.
- [9] G. Falcucci, S. Ubertini, and S. Succi. Lattice Boltzmann simulations of phase-separating flows at large density ratios: The case of doubly-attractive pseudo-potentials. *Soft Matter*, 6:4357–4365, 2010.
- [10] G. Falcucci, S. Succi, and S. Ubertini. Magnetically driven droplet break-up and vaporization: A lattice Boltzmann study. *J. Stat. Mech: Theory Exp.*, 2010:05010, 2010.
- [11] G. Falcucci, S. Ubertini, C. Biscarini, S. Di Francesco, D. Chiappini, S. Palpacelli, A. De Maio, and S. Succi. Lattice Boltzmann methods for multiphase flow simulations across scales. *Comm. Comput. Phys.*, 9(2):269–296, 2011.
- [12] G. Falcucci, M. Aureli, S. Ubertini, and M. Porfiri. Transverse harmonic oscillations of laminae in viscous fluids: a lattice Boltzmann study. *Phil. Trans. Royal Soc. A*, 369(1945):2456–2466, 2011.

- [13] M. C. Sukop and D. Or. Lattice Boltzmann method for homogeneous and heterogeneous cavitation. *Phys. Rev. E*, 71:046703, 2005.
- [14] X.-P. Chen, C.-W. Zhong, and X.-L. Yuan. Lattice Boltzmann simulation of cavitating bubble growth with large density ratio. *Comp. Math. App.*, 61(12):3577–3584, 2011.
- [15] G. Falcucci, G. Bella, S. Ubertini, S. Palpacelli, and A. De Maio. Lattice Boltzmann modeling of diesel spray formation and break-up. *SAE Int. J. Fuels Lubr.*, 3:582–593, 2010.
- [16] X. Shan and H. Chen. Lattice Boltzmann model for simulating flows with multiple phases and components. *Phys. Rev. E*, 47:1815–1820, 1993.
- [17] X. Shan and H. Chen. Simulation of nonideal gases and liquid-gas phase transitions by the lattice Boltzmann equation. *Phys. Rev. E*, 49:2941–2948, 1994.
- [18] S. Succi. *The Lattice Boltzmann Equation for Fluid Dynamics and Beyond*. Clarendon, Oxford, 2001.
- [19] P. Bhatnagar, E. Gross, and M. Krook. A model for collisional processes in gases: Small amplitude processes in charged and neutral one-component system. *Phys. Rev. Lett.*, 54, 1954.
- [20] Y. Qian, D. D’Humières, and P. P. Lallemand. Lattice BGK models for Navier-Stokes equation. *Europhys. Lett.*, 17(6):479–484, 1992.
- [21] R. Benzi, S. Succi, and M. Vergassola. The lattice Boltzmann equation: Theory and applications. *Phys. Rep.*, 222(3):145–197, 1992.
- [22] S. Zaleski, J. Li, and S. Succi. Two-dimensional Navier-Stokes simulation of deformation and breakup of liquid patches. *Phys. Rev. Lett.*, 75:244–247, 1995.
- [23] G. K. Batchelor. *An Introduction to Fluid Dynamics*. Cambridge University Press, 1967.
- [24] S. Martynov. *Numerical Simulation of the Cavitation Process in Diesel Fuel Injectors*. PhD thesis, University of Brighton, 2005.
- [25] A. Sou, S. Hosokawa, and A. Tomiyama. Effects of cavitation in a nozzle on liquid jet atomization. *Int. J. Heat and Mass Trans.*, 50(17-18):3575–3582, 2007.
- [26] G. Chiatti, O. Chiavola, and F. Palmieri. Flow features in reduced dwell time diesel injector. *SAE Tech. Paper 2008-01-0927*, 2008.
- [27] W. G. Lee and R. D. Reitz. A numerical investigation of transient flow and cavitation within minisac and VCO diesel injector nozzles. *ASME Conf. Proc.*, 643:ICES2009–76148, 2009.